CMOS-MEMS Resonator as a Signal Generator for Fully-Adiabatic Logic Circuits

Maojiao He (maojiaoh@ufl.edu), Michael P. Frank (mpf@cise.ufl.edu),
Huikai Xie (hkxie@ece.ufl.edu)
Department of Electrical and Computer Engineering, University of Florida, Gainesville, FL 32611, USA;
Phone: (352) 846-0441; Fax: (352) 846-1416

Abstract

Fully-adiabatic (thermodynamically reversible) logic is one of the few promising approaches to low-power logic design. To maximize the system power-performance of an adiabatic circuit requires an ultra low-loss on-chip clock source, which can generate an output signal with a quasi-trapezoidal (flat-topped) voltage waveform. In this paper, we propose to use high-*Q* MEMS resonators to generate the custom waveform. The big challenge in the MEMS resonator design is that a non-sinusoidal (quasi-trapezoidal) waveform needs to be generated even though the resonator oscillates sinusoidally. Our solution is to customize the shape of the sensing comb fingers of the resonator, with the result that the sensing capacitance varies quasi-trapezoidally. The effective quality factor and the area-efficiency of the microstructure have been optimized so as to minimize the whole system's power dissipation and cost at a given frequency. A resonator design with a 100 kHz resonant frequency based on a standard TSMC 0.35µm CMOS process has been fabricated. The resonator has an area of 300 µm by 160 µm with a thickness of 30 µm. Three-dimensional field simulation shows that the resonator generates a quasi-trapezoidal waveform when it operates at its resonance. An on-chip buffer is also designed for monitoring the waveform generated by the MEMS resonator. The post-CMOS fabrication process is compatible with standard CMOS processes. Thus the custom clock generator can be integrated with logic circuits on the same CMOS chip. The size of the MEMS resonator can be further reduced by design optimization and advances in micro/nano-fabrication technology.

Keyword: Fully adiabatic logic circuits, quasi-trapezoidal signal, MEMS resonator, custom comb fingers, CMOS-MEMS, High-Q

I. Introduction

The improving performance of digital electronics has been driven steadily by device scaling for over thirty years. However, device scaling is approaching its end primarily because of power dissipation constraints. Static power dissipation is mainly caused by gate current leakage arising from quantum-mechanical tunneling and source-to-drain subthreshold current leakage due to thermal excitations. These fundamental phenomena are difficult to design around. Adiabatic (or thermodynamically reversible) digital transistor-based logic circuits offer a promising alternative via architectural innovation to conventional circuitry for low power design [1]. Adiabatic logic minimizes switching energy losses by carrying out logic transitions via the gradual, adiabatic compression or expansion of the electron gas contained in a logic node. Meanwhile, standby power consumption due to leakage is minimized by keeping devices large enough so that gate-to-channel tunneling and subthreshold currents remain negligible.

To minimize the power dissipation of adiabatic logic gates, a trapezoidal (not square-wave or sinusoidal) AC power-clock voltage waveforms driving signal is required [2]. In order to keep the overall power consumption of adiabatic logic circuits low, the generation of the driving signals should also dissipate little power, i.e., a very high *Q* (quality factor) resonator is needed. Unfortunately, waveform-generation electrical circuits typically have low *Q* and incur substantial power dissipation due to the energy overhead of switching a clamping power MOSFET to limit the voltage swing of a *LC* oscillator, poor performance of integrated inductors due to low coil count and substrate coupling, and unfavorable scaling of inductor *Q* with frequency [3].

MEMS (Microelectromechanical systems) technology is an emerging technology that has a wide range of applications in automobiles, consumer electronics, communications and aerospace industries [4,5,6]. For instance, MEMS micromirrors developed by Texas Instruments, Inc. have been widely used in compact projectors and cinemas [7 8,9]. MEMS inertial sensors (i.e., accelerometers and gyroscopes) developed by Analog Devices, Inc., Robert Bosch Corp. and Motorola have been successfully used in cars for safety, drive comfort and navigation [10,11,12]., MEMS resonators with very high quality factors (above 10,000) in vacuum as well as very high resonant frequency (up into the GHz range) have been demonstrated for RF applications, such as IF filters and oscillators [5,13,14].

Mechanical structures inherently have much higher Q than electrical components. Therefore, the basic idea of this work is to use a high-Q MEMS resonator to generate the driving signals for adiabatic circuits in order to achieve overall low-power consumption. Another innovation of this work is that a trapezoidal waveform is generated by a sinusoidal oscillation of a comb drive having a special shape. Furthermore, the process used to fabricate the resonator is CMOS-compatible, so the adiabatic circuits are integrated with the trapezoidal-waveform generator on a single chip.

In this paper, first the concept of adiabatic logic circuits is introduced in Section II. Then a novel trapezoidal waveform generator using a custom designed MEMS resonator is presented in Section III. In Section IV, a 100kHz MEMS resonator design and its CMOS-compatible microfabricaton process are described.

II. Adiabatic logic circuits

Traditional digital logic electronics based on irreversible physical mechanisms dissipate roughly $\frac{1}{2}CV^2$ energy per low-level bit operation, where C is circuit node capacitance and V is the logic signal voltage. With device size and voltage scaling coming to an end in the fairly near future, the energy efficiency of these traditional mechanisms cannot continue improving much longer. Furthermore, any possible irreversible technology remains subject to the von Neumann-Landauer bound of at least $kT \ln 2$ energy dissipation per operation.

Fortunately, an alternative computing technique, *reversible computing* or *adiabatic logic*, sidesteps these energy limits, by executing a smooth, physically adiabatic transition between logical states, and can improve the performance of a typical logic circuit, given power constraints, even within a fixed technology generation. Bit energies of $\frac{1}{2}CV^2$ (and above the kT limit) are still required to be present, but rather than being dissipated on every cycle, these energies are merely transferred back and forth between logic and power supply as needed, mostly recycling their energy, except for frictional losses which can be made essentially as small as desired.

A simple reversible CMOS latch can be realized by a single standard CMOS transmission gate (T-gate). The sequence of operations shown in Figure 1 include (0) the input level is initially tied to the latch output; (1) the input changes gradually while the output follows closely; (2) the latch closes, and charge is stored dynamically (the node floats); (3) afterwards, the input signal can be removed.

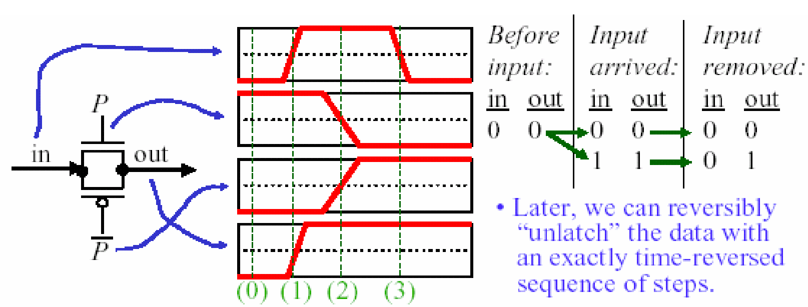

Figure 1: A simple reversible CMOS latch.

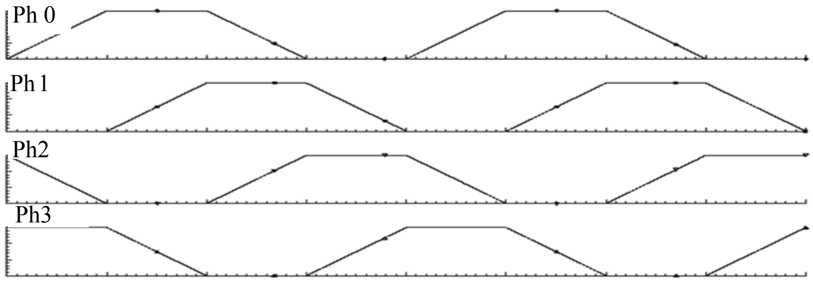

Figure 2: Clock-power supply rails for 2LAL.

In this project, we are using a simple adiabatic logic design style called 2LAL (2-level adiabatic logic) as a demonstration, which was developed at UF by one of us (Frank) in the year 2000. Like conventional CMOS, 2LAL uses two distinct voltage levels (high and low), and permits pipelined sequential circuits. It also has some very nice additional properties including: (1) Short cycle time: only 4 adiabatic transition times (*4t*) per completed clock period. (2) Low latency: only 1*t* (tick) of latency per logic level/pipeline stage. (3) Low number of supply rails: only 4 distinct driving signals need be supplied. To achieve these properties, clock/power supply rails as in Figure 2 are required. There are 4 trapezoidal voltage waveforms φ_0-φ_3, each with 50% duty cycle and 25% transition time, at relative phases of 0˚, 90˚, 180˚ and 270˚ [2].

III. MEMS resonator design

3.1 Trapezoidal Waveform Generation

The trapezoidal waveform for the adiabatic logic circuits described above will be generated by a MEMS resonator, but low-power consumption requires the MEMS resonator oscillate sinusoidally at its resonant frequency. So the challenge is that how to generate a trapezoidal waveform from a sinusoidal motion. In other words, the electrical output signal of the MEMS resonator must be saturated above a threshold displacement of the moving part of the MEMS resonator. Therefore, non-linear capacitors with a trapezoidal dependence on the resonator oscillation must be designed.

Our basic idea of designing non-linear capacitors is to use a varying gap along the travel range of the rotor to achieve the desired capacitance-position dependence. The conceptual design of one non-linear capacitor formed by an interdigitated finger pair is shown in Figure 3, in which the shapes of the rotor and stator finger have been tailored. Both stator and rotor finger have a wide flange-type end (see Fig. 3(a)). When the rotor moves along the negative y-direction, as shown in Fig. 3(b), the two fingers have no overlap and thus the sidewall capacitance formed between the fingers is

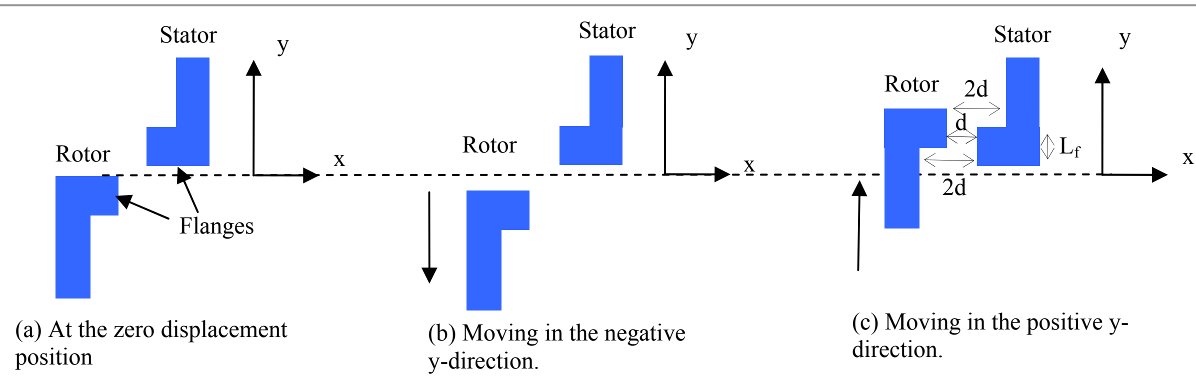

Figure 3: Conceptual design of a trapezoidal waveform generator.

very small and does not change much even with the fringing effects considered. When the rotor moves along the positive y-direction (see Fig. 3(c)), the capacitance will increase and reach its maximum when the two flanges are completely overlapped. When the rotor continues to move along the +y direction, the flange overlap decreases. However, the shifted flanges form two capacitors: one is between the rotor flange and the stator finger; and the other between the stator flange to the rotor finger. Therefore, the capacitance reduction due to the increased gap can be compensated by the dual capacitors formed between the flanges and the fingers, and thus the total capacitance can be maintained at about the maximum value even after the two flanges are no longer overlapped.

Some FEM (finite-element method) simulation results using CoventorWare [15] are shown in Fig. 4. In the simulation, three pairs of comb fingers were used. The dimensions of the comb fingers are given in Fig. 4(a), where the gap is 0.1µm, the flange width and length are 0.7/0.9µm and 0.5µm respectively, and the finger width and length are 0.5µm and 2µm, respectively. The initial separation of the rotor and stator fingers is 2.5µm, and the thickness of the entire structure is 2µm. The total comb-finger capacitance versus the rotor displacement is plotted in Fig. 4(b), which shows that the curve has a flat bottom at small displacements and a nearly saturated top at large displacements. In practice, symmetrically positioned comb pairs as the sensing combs in Figure 5(a) are often used. In those cases, the total output sensing capacitance is the superposition of two capacitances as shown in Figure 4(b), but one with a 180° phase difference. The resultant capacitance is plotted in Figure 4(c). Note that since the rotor oscillates sinusoidally the rotor moves fast around y=0, but slowly at the maximum displacements. The corresponding output electrical signal is plotted in Fig. 4(d), which as expected is a quasi-trapezoidal waveform. The waveform in Fig. 4(d) also indicates that the frequency of the output electrical signal is twice of the resonant frequency. This is due to the fact that the symmetric comb structure reaches its maximum capacitance on both +/− maximum displacements of the rotor fingers.

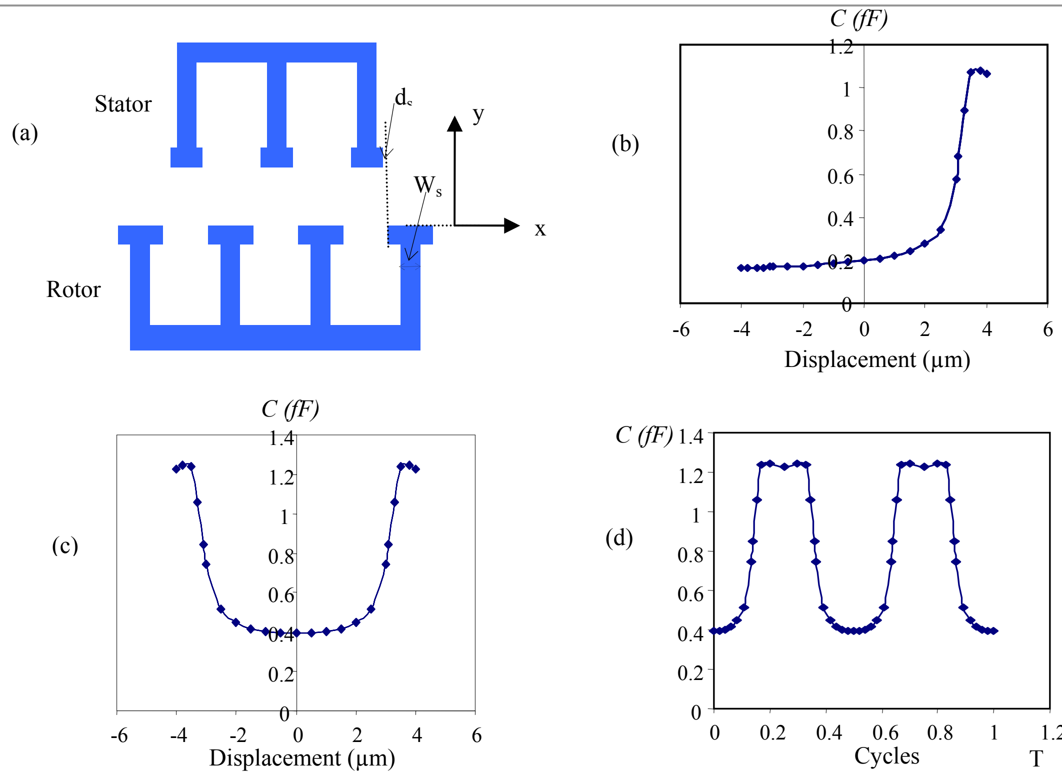

Figure 4: FEM simulation of a trapezoidal waveform generator. (a) Single side comb structure. (b) Capacitance versus the rotor displacement for single side comb structure (c) Capacitance vesus the rotor displacement for symmetric comb (superposition of two capacitances of single side comb with 180 degree phase difference (d) Quasi-trapezoidal waveform generated by symmetric comb.

3. 2 Structural design and electrostatic analysis

Beam structures are commonly used to build resonators. There are three types of resonant beam structures, clamped-clamped beams, clamped-free beams and free-free beams. Clamped-clamped beams are the most area-efficient; while free-free beams are the most energy-efficient due to reduced anchor loss [16]. Clamped-clamped beams are chosen for this design due to their simplicity and the employed fabrication process (see Section 4.1). The topology of the resonator design is shown in Fig. 5(a), where two actuation combs and four sense combs are symmetrically distributed on two sides of a clamped-clamped beam. The sense combs have exactly the same design as that shown in Fig. 4(a). A DC bias voltage V_b is applied to the central resonant beam, while a pair of DC plus AC voltages $V_c \pm v_{ac}$ are applied to the actuation combs to excite the resonator. Four sensing stators are wired together. The output nodes are at the stator fingers of the sense combs. The equivalent circuit is shown in Figure 5(b), where C_a is the actuator capacitance; C_s is the sense capacitance and C_l is the load capacitance. When the center part of the resonator is driven into resonance by the actuation combs, the rotor fingers of the sense combs will oscillate sinusoidally. In each oscillation cycle, the rotor fingers will move in and out of their stator counterparts, and generate an output signal with the same trapezoidal waveform as that shown in Fig. 4(c). Due to the high impedance at the output node, a buffer may be used to drive the bonding pads for testing purposes.

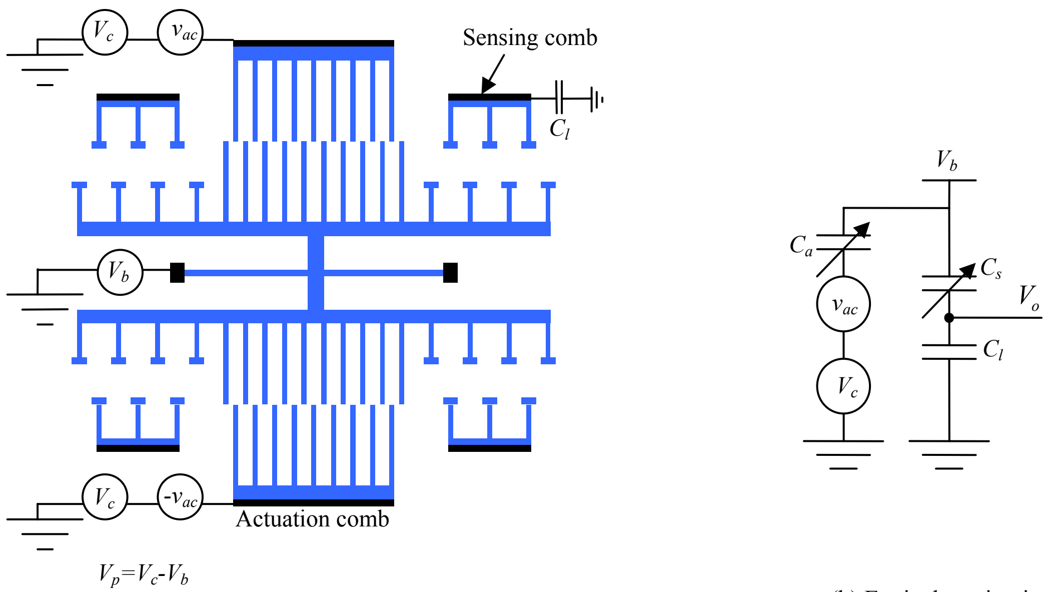

(a) The resonator design

(b) Equivalent circuit

Figure 5: The resonator topology design and electrical wiring configuration.

The static displacement of the resonator is determined by the drive force generated by the actuator and the spring constant of the central beam, i.e,,

$$x = \frac{F}{k} = \frac{1}{2k}\frac{\partial C_a}{\partial x} v_a^2 \tag{1}$$

where F is the electrostatic force, C_a is the total capacitance of the actuation combs, and k is the spring constant which is given by

$$k = 16Eh\left(\frac{W_b}{L_b}\right)^3 = M\omega^2 \tag{2}$$

where m and ω are the mass and resonant frequency of the resonator, respectively. The drive voltage of the bottom actuation comb is

$$v_a(t) = V_p + v_{ac}\sin(\omega t)\text{, where } V_p = V_b - V_c\,.$$

Therefore, the low-frequency displacement can be rewritten as

$$x = \frac{1}{2k}\frac{\partial C_a}{\partial x}\left[\left(V_P^2 + \frac{1}{2}v_{ac}^2\right) + 2V_P v_{ac}\sin(\omega t) - \frac{1}{2}v_{ac}^2\cos(2\omega t)\right] \tag{3}$$

For a high-Q resonator oscillating at its resonance (i.e., ω_r), the DC term and the second harmonic term will be suppressed. If differential voltages are applied to both sides of the actuation combs, the DC and harmonic terms will be cancelled, and the electrostatic force are doubled. Thus, the resonant displacement becomes

$$x = \frac{2Q}{k}\frac{\partial C_a}{\partial x}V_P v_{ac}\sin(\omega t) \tag{4}$$

Using the first-order approximation by neglecting fringing fields, the capacitance gradient of the actuation combs is given by

$$\frac{\partial C_a}{\partial x} \approx 2N_a\frac{\varepsilon_0 h}{d_a} \tag{5}$$

where d_a is the gap of the actuation comb fingers and N_a is the number of the stator fingers of the actuation combs.

From (2), (4) and (5), the oscillation amplitude is given by

$$X = \frac{4\varepsilon_0 h N_a Q}{k d_a}V_P v_{ac} = \frac{4\varepsilon_0 h N_a Q}{\omega^2 M d_a}V_P v_{ac} \tag{6}$$

3.3 Energy efficiency considerations

There are two important metrics that must be optimized in order to achieve low-power consumption for the adiabatic circuits. One is the effective quality factor, which is defined as the ratio of the energy transferred and the energy dissipated per clock cycle.

$$Q_{eff} = \frac{E_{tr}}{E_{diss}} \tag{7}$$

The dissipated energy, from the definition of Q, can be expressed as

$$E_{diss} = \frac{E_{total}}{Q} = \frac{M(\omega X)^2}{2Q} \tag{8}$$

The energy transferred is

$$E_{tr} = \frac{\Delta C_s V_b^2}{2} \tag{9}$$

Substituting (10) and (11) into (12) yields

$$Q_{eff} = \frac{E_{tr}}{E_{diss}} = \frac{Q\Delta C_s V_b^2}{M(\omega X)^2} \tag{10}$$

The dissipated energy is affected by the unloaded quality factor, spring constant and vibration amplitude of the resonator. The major energy dissipation mechanisms include air damping, clamping loss through the substrate, thermoelastic damping, electronic damping, surface loss and intrinsic material losses [17][18]. Air damping can be minimized by using vacuum packaging. Clamping losses to the substrate can be avoided by locating the support at a nodal point of the vibration mode or using impedance-mismatched supports to reflect energy back [16]. Thermoelastic dissipation (heat flow resulting from nonuniform strain) can be reduced by shrinking device size, using stiff, high thermal conductivity materials (Si, diamond) [19] or utilizing modes with uniform compression/expansion [20]. Surface loss mechanisms can be minimized by avoiding layered structures (thin-film interfaces) at surfaces. Intrinsic material losses make designers prefer single-crystal materials. All these damping mechanisms are intrinsic factors that limit unloaded Q, and thus the corresponding Q_{eff} . The extrinsic factors that limit Q_{eff} are the applied voltage, vibration amplitude, mass of the resonator, and resonance frequency.

The other important metric is the area energy transfer efficiency α_E, which is defined as the ratio between the energy transferred and the area consumed by the resonator, i.e.,

$$\alpha_E = \frac{E_{tr}}{Area} = \frac{\Delta C_s V_b^2}{2\times Area} \tag{11}$$

This efficiency affects the cost overhead of the adiabatic solution. From (10) and (1113), it is clear that high DC voltage, small mass and small vibration amplitude are desired. However, the maximum DC voltage can be applied here is limited by the oxide breakdown and air breakdown voltages. For a resonator gap size as small as 0.1 µm, the air breakdown voltage is approximately 110 V per µm of air gap [21]. Simulation shows that sufficient displacements can be achieved at $V_P = 10V$. So, the maximum applied voltage in this case is about $10V$. The output voltage V_o can be much smaller than $10V$, depending on the load capacitance, and will be tuned to the transistor operating voltage. The resonator size and resonance frequency are defined by the system requirements. The sensing capacitance is approximately proportional to the mass. So the mass should not be too small. The vibration amplitude is determined by the maximum voltage, fabrication accuracy and the waveform realization mechanism.

Note in Figure 4(c), the sense capacitance swing is very small, only ~0.2 fF per comb finger. However, it should be feasible to increase the structure thickness by a factor of 20 using a DRIE process to yield a figure close to 4 fF per comb finger. Using a bias voltage of 10 V, this means each comb finger could drive a load equivalent to about 40 minimum sized devices of about 1 fF load capacitance each, through a voltage swing of ~1V. The area needed for this many devices is comparable to the area occupied by the comb fingers. Table 1 shows some key parameters of a prototype resonator with a 0.5 MHz resonant frequency. The unloaded Q factor is estimated as 5000 according to the employed fabrication technology.

Table 1: Key parameters of a 0.5 MHz resonator

Thickness:	2 µm	Bias voltage V_b:	10 V
Gap size:	0.1 µm	DC drive voltage $\|V_c-V_b\|$:	10 V
Finger width:	0.5 µm	AC drive voltage v_{ac}:	0.2 V
# of actuation fingers N_a:	40	Area A:	107 µm ×36 µm
# of sensing fingers N_s:	106	Capacitance variation:	20 fF
Quality factor Q:	5000 (est.)	Effective quality factor Q_{eff}:	46
Vibration amplitude X:	4 µm	Area efficiency α_E	3.23×10^{-4} J/m^2

3.4 A Special Actuation Comb Design

Smaller gaps can significantly improve the actuation and sensing efficiency, which in turn increase the effective quality factor. The smallest gap size is determined by the fabrication technology. For instance, to etch 50µm-deep trenches in silicon, the minimum gap size should be 2µm for a 25:1 aspect-ratio DRIE process. One technique that can overcome this limitation is illustrated in Fig. 6, where all fingers have narrowed tips. The narrowed tips guarantee the minimum initial gaps for microstructure release. After the small initial displacement, the comb fingers are engaged with a much reduced gap which can be as small as 0.1 µm.

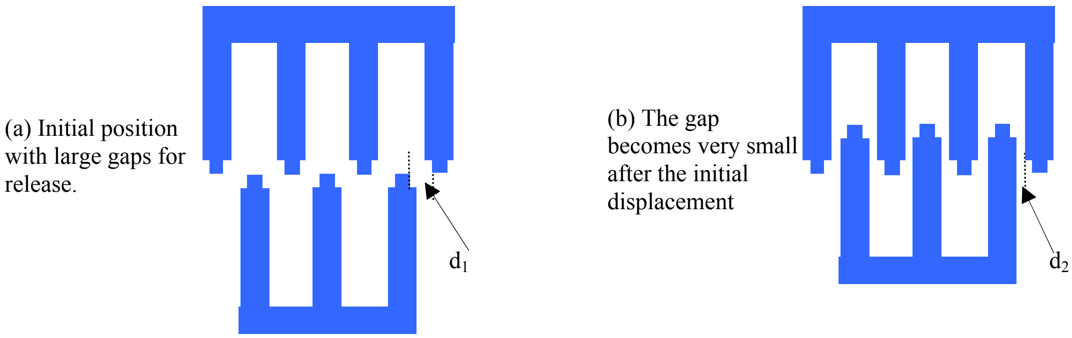

Figure 6: A comb drive design for achieving small effective gap sizes. $d_2 << d_1$

IV. An Implemented Resonator Prototype

4.1 DRIE CMOS-MEMS Process

A maskless post-CMOS micromachining process is used to fabricate the proposed MEMS resonator [22]. The fabrication requires only dry-etch steps and is completely CMOS-compatible so that electronics can be integrated on the same chip with MEMS structures. The CMOS chips are fabricated using a commercial 4-metal CMOS technology through MOSIS [23]. The post-CMOS micromachining process starts with the backside etching to define a 50µm-thick silicon membrane (Fig. 7(a)). Then anisotropic SiO_2 etching is performed to expose the regions for electrical isolation of silicon (Fig. 7(b)). Then the top metal layer is removed (Fig. 7(c)). Next, a deep silicon etch followed by an isotropic silicon etch is performed to undercut the silicon underneath the isolation beams (Fig. 7(d)), which isolates sense comb fingers from each other and from silicon substrate. Next, the second anisotropic SiO_2 etch defines sense comb fingers, springs and other mechanical structures (Fig. 7(e)). Finally, a deep silicon etch is performed again to etch through and release the resonator (Fig. 7(f)).

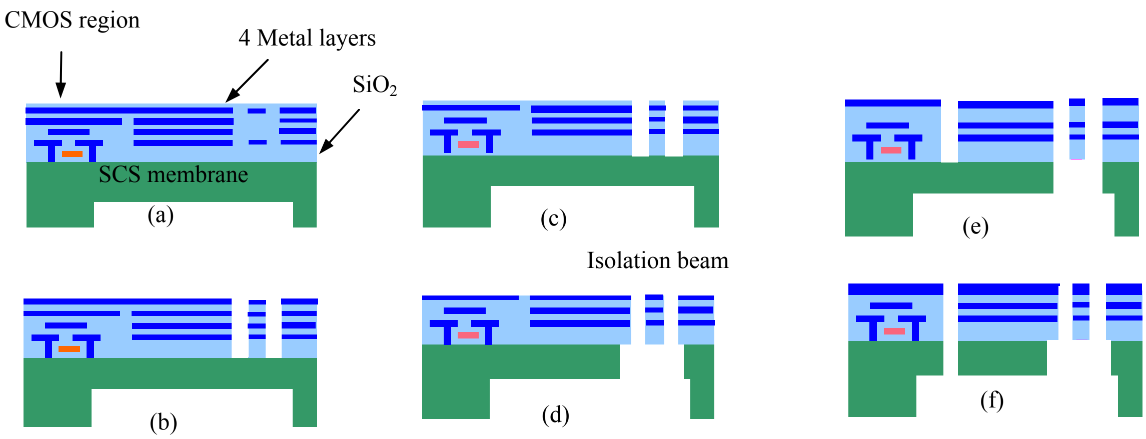

Figure 7: (a) Backside etch. (b) Anisotropic SiO_2 etch (c) Top Al etch. (d) isotropic deep Si etch followed by Si undercut. (e) Anisotropic SiO_2 etch. (f) Anisotropic deep Si etch

4.2 A prototype 100kHz resonator design

The design was based on the TSMC 4-metal 0.35µm CMOS process. The top metal layer (metal-4) is laid out as the etching mask for electrical isolation of silicon. Metal-3 defines the resonator structure. Metal-1 and metal-2 are used for electrical wiring. Fig. 8(a) shows the 3D model of the resonator generated by CoventorWare [15]. Fig. 8(b) is the side view showing the silicon undercut for electrical isolation. The key parameters of this design are listed in Table 2.

The main objective of this design is to verify the generation of trapezoidal waveforms, so the resonant frequency is targeted at 100 kHz. Even though the area of this design is much larger than that of the design listed in Table 1, the gap is larger and thus the DC bias voltage can be higher. Therefore, the effective quality factor is just reduced by a factor of 3 down to 15. Figure 9 shows a scanning electron micrograph (SEM) of a released resonator. The device is under testing.

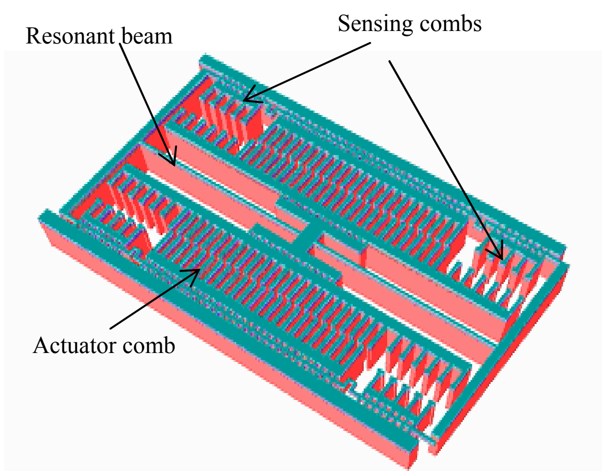

(a) 3D model

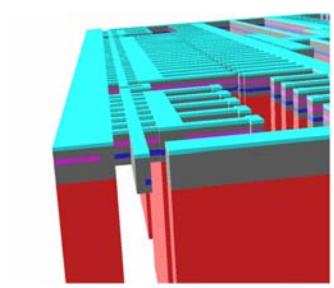

(b) Electrical isolation of silicon

Figure 8: The 3D model of the resonator.

Table 2**:** Key parameters of a prototype resonator at 100 kHz

Thickness:	30 μm	Bias voltage V_b:	10 V
Gap size:	0.5 μm	DC drive voltage $\|V_c-V_b\|$:	30 V
Finger width:	2.5 μm	AC drive voltage v_{ac}:	2 V
# of actuation fingers N_a:	48	Area A:	260 μm ×130 μm
# of sensing fingers N_s:	24	Capacitance variation:	30 fF
Quality factor Q:	5000 (est.)	Effective quality factor Q_{eff}:	15
Vibration amplitude X:	16 μm	Area efficiency α_E	1×10^{-4} J/m^2

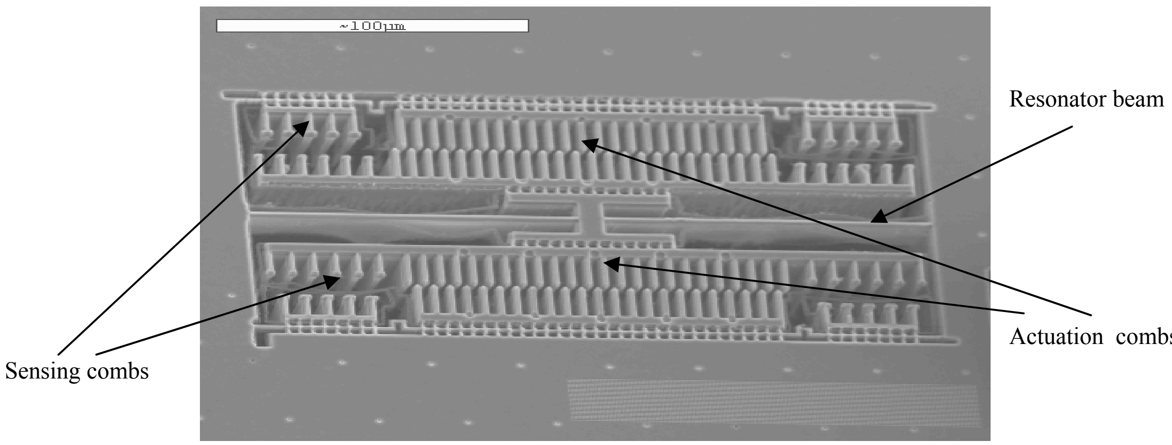

Figure 9: SEM picture of the resonator

V. Conclusion

A trapezoidal waveform generator is realized by customizing the shape of the sensing comb fingers of a MEMS resonator. A resonator design with a 100 kHz resonant frequency has been fabricated. The fabrication process is compatible with standard CMOS processes and thus the MEMS resonator can be integrated with logic circuits on the same CMOS chip. The size of the MEMS resonator can be further reduced by design optimization and advances in micro/nano-fabrication technology. Using the same principle, other custom waveforms can also be generated from sinusoidal oscillations.

Acknowledgements

The authors would like to thank Hongwei Qu for the help in the MEMS fabrication and SEM. This project is supported by the Semiconductor Research Corporation.

REFERENCES

1 Lars Svensson. "Adiabatic and clock-powered circuits." In Christian Piguet (ed): *Low-Power Electronics Design.* Chapter 15. CRC Press, 2004. ISBN 0849319412.

2 Venkiteswaran Anantharam, Maojiao He, Krishna Natarajan, Huikai Xie, Michael P. Frank, "Driving Fully-Adiabatic Logic Circuits Using Custom High-*Q* MEMS Resonators," *presented at the 2004 workshop on Methodologies for Low Power Design*, part of the ESA '04 (Embedded Systems and Applications) conference, held in Las Vegas, Nevada, June 21-24, 2004.

3 Matthew E. Becker and Thomas F. Knight, Jr., "Transmission Line Clock Driver," in *Power Driven Microarchitecture Workshop*, pp. 80-85, held in Barcelona, Spain, 28 June 1998.

4 Takeda, M.; **"**Applications of MEMS to industrial inspection" *Micro Electro Mechanical Systems*, 2001, MEMS2001. The 14th IEEE International Conference on , 21-25 Jan 2001 Pages:182 - 191

5 Clark T.-C. Nguyen, "MEMS Technologies for Communications," in *NanoTech 2003: Technical Proceedings of the 2003 Nanotechnology Conference and Trade Show*, held Feb. 23-27, 2003, San Francisco, CA, vol. 1, pp. 452-455, Computational Publications, Boston.

6 Gabriel, K.J., **"**Microelectromechanicalsystems(MEMS)" *Aerospace Conference,* IEEE, Volume:3, 18 Feb.1997 Pages:9 - 43 vol.3

7 http://www.dlp.com/dlp_technology/dlp_technology_overview.asp?bhcp=1

8 Hornbeck,L.J., "Digital Light Processing and MEMS: an overview", *Advanced Applications of Lasers in Materials Processing,* 1996/Broadband Optical Networks/Smart Pixels/Optical MEMs and Their Applications, 1996. IEEE/LEOS 1996 Summer Topical Meetings: , 5-9 Aug. 1996

9 Ohara, K.; Kunzman, A.; "Video processing technique for multimedia HDTV with digital micro-mirror array", *Consumer Electronics, IEEE Transactions* on , Volume: 45 , Issue: 3 , Aug. 1999

10 http://www.analog.com/en/cat/0%2C2878%2C764%2C00.html

11 http://www.europractice.bosch.com/en/mst/index.htm

12 Hammond, J.; McNeil, A.; August, R.; Koury, D., "Inertial transducer design for manufacturability and performance at Motorola", *TRANSDUCERS, Solid-State Sensors, Actuators and Microsystems,* 12th International Conference on, 2003 , Volume: 1 , 8-12 June 2003

13 Aigner, R.; Ella, J.; Timme, H.-J.; Elbrecht, L.; Nessler, W.; Marksteiner, S,"Advancement of MEMS into RF-filter applications"**,** *Electron Devices Meeting, 2002. IEDM '02. Digest.* International , 8-11 Dec. 2002

14 Sukhan Lee; Chungwoo Kim; Sunghwan Jung; In-Sup Song; Yong Chul Cho, "MEMS for IT applications" *Micromechatronics and Human Science, 2001*. MHS 2001. Proceedings of 2001 International Symposium on , 9-12 Sept. 2001

15 http://www.coventor.com

16 K. Wang, Y. Yu, A.-C. Wong, and C. T.-C. Nguyen, "VHF free-free beam high-*Q* micromechanical resonators," *Technical Digest, 12th International IEEE Micro Electro Mechanical Systems Conference,* Orlando, Florida, Jan. 17-21, 1999, pp. 453-458.

17 Rob N. Candler, Huimou Li, Markus Lutz, Woo-Tae Park, Aaron Partridge, Gary Yama and Thomas Q. Kenny, "Investigation of Energy Loss Mechanisms in Micromechanical Resonators", *The 12th International Conference on Solid State Sensors, Actuators and Microsystems,* Boston, June 8-12, 2003

18 Amy Duwel, John Gorman, Marcie Weinstein, Jeff Borenstein, Paul Ward, "Experimental Study of Thermoelastic Damping in MEMS Gyros", Sensors and Actuators A 103 (2003) 70-75

19 Srikar, V.T.; Senturia, S.D, "Thermoelastic damping in fine-grained polysilicon flexural beam resonators', *Microelectromechanical Systems, Journal of ,* Volume: 11 , Issue: 5 , Oct. 2002, Pages:499 - 504

20 S. Pourkamali, A. Hashimura, R. Abdolvand, G. K. Ho, A. Erbil, and F. Ayazi, "High-Q Single Crystal Silicon HARPSS Capacitive Beam Resonator With Self-Aligned Sub-100-nm Transduction Gaps", *JOURNAL OF MICROELECTROMECHANICAL SYSTEMS,* VOL. 12, NO. 4, AUGUST 2003

21 P.G. Slade, E.D. Taylor, **"**Electrical Breakdown In Atmospheric Air Between Closely Spaced (0.2µm-40µm) Electrical Contacts", *Proceedings of the Forty-Seventh IEEE Holm Conference on Electrical Contacts*, Sept. 10-12, 2001, pp. 245–250.K.

22 H H. Xie, L. Erdmann, X. Zhu, K. Gabriel and G. Fedder, "Post-CMOS Processing For High-aspect-ratio Integrated Silicon Microstructures", *Journal of Microelectromechanical Systems,* Vol. 11, no. 2, 2002, pp.93-101.

23 http://www.mosis.org